RSC Advances

PAPER

View Article Online
View Journal | View Issue

Cite this: *RSC Adv.*, 2025, **15**, 50053

Tri-layer structured intelligent hydrogel dressing for controlled-release antibacterial treatment of chronic diabetic wounds

Weikai Zhang, *[abc] Xiuhong Fu,[de] Hewei Zhang,[a] Shaozhe Zhang,[de] Qingwei Zhang,[de] Chongkai Zhai,[a] Jinyang Zhao,[abc] Quanzhong Yang[abc] and Shuang Li[abc]

Chronic diabetic wounds are notoriously difficult to heal due to a hyperglycemic environment, persistent oxidative stress, and infection, leading to slow healing and frequent complications. In this study, we developed a tri-layer intelligent hydrogel dressing for diabetic wound care. The top layer contains silver nanoparticles (AgNPs) for rapid initial antibacterial action. The middle layer incorporates poly(lactic-*co*-glycolic acid) (PLGA) microspheres loaded with mangiferin to achieve sustained drug release and promote angiogenesis. The bottom layer is a gelatin methacryloyl (GelMA) hydrogel scaffold that provides structural support. The composite materials' morphology and structure were characterized by scanning and transmission electron microscopy (SEM, TEM). We evaluated the properties of hydrogel contain mechanical properties, degradation and swelling behaviors, drug release profiles, antibacterial and antibiofilm effects, and cell-related biological properties. The results showed that the tri-layer hydrogel exhibited higher mechanical strength and greater degradation stability than a homogeneous GelMA hydrogel. The layered structure of hydrogel effectively delayed the release of mangiferin, resulting in a significantly lower cumulative release over 72 hours compared to a non-layered control. Antibacterial tests demonstrated that the tri-layer hydrogel produced the largest inhibition zones and the highest bacterial-killing rates against *Staphylococcus aureus* (*S. aureus*) and *Escherichia coli* (*E. coli*), and it markedly inhibited the formation of bacterial biofilms. *In vitro*, cell studies showed that the tri-layer hydrogel significantly downregulated the pro-inflammatory cytokines IL-6 and TNF-α, upregulated the anti-inflammatory cytokine IL-10, and substantially reduced intracellular reactive oxygen species (ROS) accumulation. In summary, the tri-layer intelligent hydrogel dressing, through its synergistic controlled-release and antibacterial mechanisms, offers an effective multi-factorial intervention strategy for the treatment of chronic diabetic wounds.

Received 12th September 2025
Accepted 7th December 2025

DOI: 10.1039/d5ra06906h

rsc.li/rsc-advances

Introduction

Diabetic chronic wounds, particularly diabetic foot ulcers (DFUs), are among the most common and disabling complications in diabetic patients.[1] Under prolonged hyperglycemic conditions, diabetic wounds face a complex pathological microenvironment. This includes impaired local microcirculation, immune dysfunction, persistent inflammation, and bacterial infection. These factors collectively lead to elevated oxidative stress, abnormal macrophage polarization, and restricted angiogenesis at the wound site. Consequently, these dysfunctions significantly hinder the healing process.[2,3] Statistics indicate that more than 15% of diabetic patients will develop foot ulcers during their lifetime, with approximately 14% to 25% eventually requiring amputation, severely compromising patients' quality of life and survival rate.[4] Therefore, the development of multifunctional intelligent wound dressings (integrating antibacterial, anti-inflammatory, and tissue-repairing properties) has become a crucial research focus in the treatment of diabetic chronic wounds.[5,6]

Hydrogels, as representative biomimetic moist dressings, exhibit significant advantages in chronic wound management due to their high-water content (providing a moist healing environment), excellent biocompatibility, injectability, and tunable 3D network structure.[7–9] In recent years, functional hydrogels have evolved toward multi-layered and multifunctional systems,

[a]*Institute of Medical Technology, Luoyang Polytechnic, Luoyang, 471000, China. E-mail: 202110008@lypt.edu.cn*

[b]*Henan Engineering Research Center of Key Immunological Biomaterials, Luoyang Polytechnic, Luoyang, 471000, China*

[c]*Zhongyuan Scholars Workstation of Henan, Luoyang Polytechnic, Luoyang, 471000, Henan, China*

[d]*Henan Key Laboratory of Fertility Protection and Aristogenesis, Luohe Central Hospital, Luohe , 462000, China*

[e]*Gynecology and Obstetrics Department, Luohe Central Hospital, Luohe , 462000, China*

enabling targeted therapeutic strategies through structural layering or synergistic multi-component action.[10–12] Among them, controlled drug release and responsiveness to the wound microenvironment are key techniques to enhance the therapeutic efficacy for diabetic chronic wounds.[13–16]

Mangiferin, a natural polyphenolic flavonoid compound derived from mango leaves, possesses strong antioxidant capacity, significant anti-inflammatory properties, and the ability to promote angiogenesis. It has demonstrated broad potential in repairing tissue damage caused by oxidative stress and inflammatory imbalance.[17–19] However, its poor water solubility and rapid inactivation *in vivo* limit its sustained efficacy in the wound microenvironment.[20] Therefore, this study utilized poly(lactic-*co*-glycolic acid) (PLGA) to construct a sustained-release delivery system for mangiferin. PLGA, an FDA-approved biodegradable polymer, offers excellent biosafety and controlled-release properties, and has been widely used in the preparation of small-molecule drug microspheres.[21] Mangiferin-loaded PLGA microspheres were prepared *via* the emulsion solvent evaporation method, yielding a carrier platform with controllable particle size and high drug encapsulation efficiency.

Moreover, early-stage infection control is vital for effective healing of chronic wounds.[5,22] Silver nanoparticles (AgNPs), owing to their broad-spectrum antibacterial activity, low likelihood of inducing bacterial resistance, and controllable cytotoxicity, are commonly incorporated into hydrogel systems to impart antibacterial functionality.[23–25] AgNPs continuously release Ag^+ ions, which interfere with bacterial protein synthesis and disrupt membrane structures. This mechanism enables them to significantly inhibit both Gram-positive and Gram-negative bacteria, thereby effectively reducing wound bacterial load and biofilm formation.[26,27]

While multifunctional hydrogels have been extensively explored for diabetic wound healing, our three-layer structured design offers distinct advantages over the prevalent strategies in existing literature, which primarily include single-layer homogeneous composites or simpler bilayer systems.[28–30] Single-layer systems, where multiple functional components are simply blended, often face challenges in independently controlling release kinetics and risk functional interference such as Ag^+ potentially inactivating sensitive therapeutic agents. Bilayer systems, typically featuring a top antibacterial layer and a bottom pro-healing layer, represent an advancement but often lack the granularity for sophisticated temporal control required for the protracted healing phases of diabetic wounds.[7,29]

Based on the above therapeutic needs and material characteristics, this study designed and constructed a three-layer structured intelligent hydrogel wound dressing system. The upper layer is rich in AgNPs to rapidly combat bacterial infection; the middle layer contains mangiferin-loaded PLGA microspheres to scavenge oxidative stress and promote sustained angiogenesis; the bottom layer uses gelatin methacrylate (GelMA) as the base to provide support and biocompatibility.[31–33] In contrast to previous study, our tri-layer hydrogel uniquely utilizes a layered architecture to spatially separate and sequentially release different therapeutic agents. This stratified approach offers distinct advantages in controlling release kinetics and reducing interferences between components. This composite hydrogel integrates key features including injectability, mechanical support, sustained release, and multimodal antibacterial properties. It is designed to synergistically address the complex barriers in diabetic chronic wound healing, thereby providing a targeted, high-biofunctionality, material-based strategy for next-generation wound management systems.

Materials and methods

Materials and reagents

Gelatin methacrylate (GelMA) was synthesized *via* reaction of gelatin (Type A, 300 Bloom, Sigma-Aldrich, USA) with methacrylic anhydride (MA, Aladdin, China) at 50 °C for 2 h. The product was purified by dialysis and lyophilized. Mangiferin (purity ≥98%) was purchased from Chengdu Mansite Biotechnology Co., China. PLGA (lactide: glycolide = 50 : 50, MW ≈ 20 000–50,000 Da, Evonik, Germany) was used for the drug release carrier. AgNPs were synthesized *via* chemical reduction: silver nitrate (Sinopharm, China) was reduced by trisodium citrate (Aladdin, China) at 100 °C to obtain stable AgNPs (50 nm).[34,35] Irgacure 2959 (Sigma-Aldrich, USA) was used as the photoinitiator.[36] Ultrapure water was from a Milli-Q system (Millipore, USA). All other reagents were analytical grade (Sinopharm or Aladdin) and used without further purification.

L929 fibroblasts(Cat. No. 06.0372), RAW264.7 macrophages (Cat. No. 06.0255) and Human umbilical vein endothelial cell lines (HUVECs) (Cat. No. 06.0650) were purchased from Eallbio life sciences, Beijing China. Primary antibodies anti-CD86 (Cat. No. 105001) was purchased from BioLegendand, and anti-CD206 (Cat No. 98031-1-RR) was obtained from Proteintech Group, China. The fluorophore-conjugated secondary antibodies were purchased from Jack & ImmunoResearch Inc. USA.

Mangiferin-loaded PLGA microspheres were fabricated using an emulsion-solvent evaporation technique.[37] Briefly, the PLGA (200 mg) and mangiferin (20 mg) were dissolved in 4 mL of dichloromethane to form the organic phase. This organic solution was then added dropwise into 40 mL of an aqueous phase containing 2% (w/v) poly(vinyl alcohol) (PVA) under continuous magnetic stirring at 500 rpm (magnetic stirrer). The mixture was immediately emulsified using a probe ultrasonicator (Scientz JY92-IID) at 20% amplitude for two 30 seconds pulses to form a stable oil-in-water (O/W) emulsion. Subsequently, the emulsion was stirred at 500 rpm for approximately 3 hours at room temperature to allow for complete solvent evaporation and microsphere solidification. The resulting microspheres were collected by centrifugation at 8000×*g* for 5 minutes, washed three times with distilled water to remove residual PVA, and finally lyophilized to obtain the dry powder. The mangiferin@PLGA microspheres were stored under light-protected and dry conditions for further use.

Hydrogel fabrication and group design

GelMA hydrogels were prepared by UV crosslinking. A 10% (w/v) GelMA prepolymer solution was made by dissolving GelMA in

PBS and adding 0.5% (w/v) Irgacure 2959. This solution was fully dissolved at 37 °C and then filtered to sterilize. Four hydrogel groups were designed for comparison.

Group A (blank GelMA). Pure GelMA hydrogel without any functional additives, serving as a blank control to assess the baseline properties of the GelMA matrix.

Group B (mangiferin@PLGA). GelMA prepolymer solution uniformly dispersed with a certain concentration of mangiferin@PLGA microspheres, followed by UV crosslinking to form a homogeneous composite hydrogel. This group provides only the sustained release of mangiferin and is used to evaluate the effect of a single drug-release component.

Group C (AgNPs + mangiferin). GelMA prepolymer solution directly mixed with a silver nanoparticle solution and an equivalent amount of free (unencapsulated) mangiferin, then UV crosslinked. This group contains an antibacterial component and free drug but no sustained-release carrier, used to study the direct synergistic effect of AgNPs and free mangiferin.

Group D (tri-layer structure). A three-layer hydrogel was fabricated by sequential casting as shown in Fig. 1. First, a GelMA prepolymer solution containing AgNPs was poured into a mold to form the top layer and briefly exposed to 365 nm UV light for initial crosslinking. Next, a GelMA prepolymer solution containing mangiferin@PLGA microspheres was carefully added to form the middle layer and UV crosslinked again. Finally, pure GelMA prepolymer was added to form the bottom layer, and the entire construct was fully UV crosslinked. The resulting tri-layer hydrogel has an AgNP-rich top layer, a middle layer with mangiferin-loaded microspheres, and a pure GelMA scaffold bottom layer.

All prepared hydrogels were fully crosslinked under 365 nm UV light for 30–60 seconds and then equilibrated in PBS before further testing.

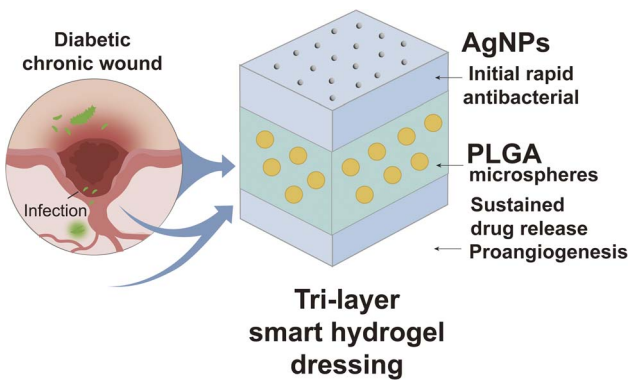

Fig. 1 Schematic illustration of a three-layered intelligent hydrogel dressing for diabetic chronic wound healing. The diagram highlights the pathological features of diabetic chronic wounds, including persistent infection and impaired angiogenesis. The designed dressing consists of three functional layers: (1) a top layer loaded with silver nanoparticles (AgNPs) for initial rapid antibacterial activity; (2) a middle layer incorporating PLGA microspheres for sustained drug release; and (3) a bottom hydrogel layer promoting angiogenesis to enhance tissue regeneration.

Characterization and testing methods

Morphology observation

The freeze-dried PLGA microspheres were adhered to conductive tape, sputter-coated with gold, and observed under scanning electron microscopy (SEM; Hitachi SU8010, Japan) at 10 kV to assess their surface morphology and particle size. Some microspheres were suspended in absolute ethanol, a drop placed on a copper grid with carbon film, dried naturally, and then observed by transmission electron microscopy (TEM; JEOL JEM-2100, Japan) to examine their internal structure. Hydrogel samples were freeze-dried, fractured in liquid nitrogen to expose cross-sections, sputter-coated with gold, and observed by SEM to analyze their porous structure and interlayer interfaces. PLGA Microsphere Size: Lyophilized PLGA microspheres were suspended in deionized water and sonicated briefly to disperse aggregates. Particle size distribution was measured by dynamic light scattering (DLS) using a Zetasizer Nano ZS instrument (Malvern, UK).

Chemical structure analysis

Hydrogel samples from each group were freeze-dried, ground into powder, and scanned by Fourier-transform infrared spectroscopy (FTIR; Thermo Nicolet iS10, USA) over the range 4000–500 cm^{-1} to analyze characteristic functional group peaks. Some samples were dissolved in DMSO-d_6 and analyzed by proton nuclear magnetic resonance (^1H NMR; Bruker AVANCE III 400 MHz, Germany) to confirm the incorporation of mangiferin and PLGA into the GelMA network.

Mechanical testing

Prepared cylindrical hydrogels (10 mm diameter, 5 mm height) were placed between the platens of a universal testing machine (Instron 5943, USA). The samples were compressed at a rate of 2 mm min^{-1} up to 60% strain, and the stress–strain curves were recorded. The compression modulus was calculated from the slope of the linear elastic region of the stress–strain curve.

In vitro degradation

Freeze-dried hydrogel samples were weighed to obtain the initial dry weight (W_0) and immersed in PBS (pH 7.4) containing 0.02% sodium azide at 37 °C. At 1, 2, 3, 4 and 5 days, samples were retrieved, rinsed with PBS, freeze-dried, and weighed to obtain the residual dry weight (W_t). The remaining mass percentage ($W_t/W_0 \times 100\%$) was calculated to determine degradation rate, and degradation curves were plotted.

Swelling behavior

Dried hydrogel samples were placed in PBS at 37 °C and incubated for 10, 30, 60, 120, 240 and 360 minutes. At each time point, samples were removed, surface moisture blotted off with filter paper, and the swollen weight (W_s) measured. The swelling ratio was calculated as $(W_s - W_0)/W_0 \times 100\%$, and swelling kinetics curves were plotted.

Drug release study

Hydrogels loaded with mangiferin were incubated in PBS at 37 °C in a shaking incubator (Thermo MaxQ 4000, USA). At 1, 4, 8, 12, 24, 48, and 72 hours, aliquots of the supernatant were collected and replaced with an equal volume of fresh PBS. The concentration of mangiferin in the collected supernatant was determined by UV-visible spectrophotometry (Shimadzu UV-2600, Japan) at 256 nm, using a pre-established standard curve to calculate cumulative release percentage.

Drug release kinetics

The cumulative release data were fitted to various kinetic models (zero-order, first-order, Higuchi, Korsmeyer-Peppas, Peppas-Sahlin, and Hixson-Crowell) using curve-fitting tools in GraphPad Prism 9.0. Model fit quality was assessed by the coefficient of determination (R^2) and the root-mean-square error to determine the predominant release mechanism.

Antibacterial performance testing

Inhibition zone measurement

The agar diffusion method was used. Hydrogel samples were tested at 20 mg mL^{-1} (w/v) against two model bacteria: *Staphylococcus aureus* (*S. aureus,* ATCC 25923) and *Escherichia coli* (*E. coli*, ATCC 25922). Bacterial suspensions were prepared in nutrient broth at an initial inoculum of 5×10^5 colony-forming units (CFU) per mL. Hydrogel disks (6 mm diameter) from each group were placed on the agar surface with a lawn of bacteria suspension. Plates were incubated at 37 °C for 24 hours, after which the diameters of the inhibition zones were measured.

Colony counting

Each hydrogel sample was incubated with a standardized bacterial suspension for 4 hours. After co-incubation, the bacterial suspension was diluted serially (10-fold dilutions) and plated on nutrient agar. Plates were incubated overnight at 37 °C, and colony-forming units (CFU) were counted using a colony counting analyzer (Interscience Scan 500, France).

Live/dead staining

After 4 hours of co-culture, bacterial suspensions were stained using the LIVE/DEAD® BacLight™ Bacterial Viability Kit (Invitrogen, USA) and observed under a fluorescence microscope (Nikon Eclipse Ti2, Japan) to distinguish live (green) and dead (red) bacteria.

Biofilm inhibition

Hydrogel extracts were added to wells of a 96-well plate, with plain culture medium as control, and co-incubated with bacterial (*E.coli*) suspensions for 24 hours. Planktonic cells were gently washed off with PBS, and the remaining biofilm was stained with 0.1% crystal violet for 15 minutes. The stain was eluted with 95% ethanol, and the optical density (OD_{595}) was measured with a microplate reader (BioTek Synergy HTX, USA) at 595 nm to quantify residual biofilm biomass.

Cell studies

L929 fibroblasts were seeded in 24-well plates. After overnight culture, cells were treated with hydrogel extracts for 24 hours. The levels of pro-inflammatory cytokines IL-6 and TNF-α and the anti-inflammatory cytokine IL-10 in the supernatants were measured using ELISA kits (MultiSciences, Hangzhou) to evaluate the material's effect on macrophage inflammatory factor secretion. Intracellular ROS levels were detected using the fluorescent probe DCFH-DA (Beyotime, Shanghai). After staining, cells were observed under a fluorescence microscope to visualize green fluorescence intensity, and fluorescence was quantitatively measured with a multi-mode microplate reader (Tecan Infinite M200 Pro, Switzerland) at $E_x/E_m = 488/525$ nm. All cell experiments were performed in at least triplicate, and statistical analysis was used to assess significance.

Immunofluorescence staining

RAW264.7 macrophages were seeded on glass coverslips in 24-well plates and incubated with hydrogel extracts (GelMA, GelMA/PLGA, Mang, Trilayer) for 24 h. Cells were then washed with PBS and fixed in 4% paraformaldehyde for 15 min at room temperature. After washing, cells were permeabilized with 0.3% Triton X-100 and blocked with 5% bovine serum albumin for 60 min. Cells were incubated overnight at 4 °C with primary antibodies against CD206 and CD86 (diluted in blocking buffer), followed by washing and incubation with fluorophore-conjugated secondary antibodies for 1 h at room temperature. Finally, nuclei were counterstained with DAPI dye, coverslips were mounted on slides, and immunofluorescence images were acquired on a fluorescence microscope using standard filter sets.

Tube-formation assay

Endothelial tube formation was evaluated using a Matrigel-based assay. Growth factor-reduced Matrigel (Corning) was thawed on ice and 100 μL was added to each well of a pre-chilled 96-well plate. The plate was incubated at 37 °C for 30 min to allow the Matrigel to polymerize. Human umbilical vein endothelial cells (HUVECs) were harvested, resuspended in endothelial growth medium, and seeded onto the solidified Matrigel at a density of 2×10^4 cells per well. For treatment, the culture medium was supplemented with the corresponding hydrogel extracts (GelMA, GelMA/PLGA, Mang, or Trilayer). Cells were incubated at 37 °C, 5% CO_2 for 6 h to allow tube formation. At the end of the incubation, the tubular networks were observed and imaged using an inverted phase-contrast microscope.

Statistical analysis

All quantitative data are presented as mean ± standard deviation (SD). Experiments were performed in triplicate ($n = 3$) or more as indicated. Statistical comparisons were conducted using GraphPad Prism 9. For comparisons among multiple groups (≥3 group), one-way analysis of variance (ANOVA) was performed, followed by Tukey's post hoc test for pairwise comparisons. For time-course data, we used two-way ANOVA

when comparing two different formulations over time, with appropriate post hoc analysis. A value of $p < 0.05$ was considered statistically significant. Significance levels in figures are indicated as $*p < 0.05$ (single asterisk), $**p < 0.01$ (double asterisks), $***p < 0.001$ (triple asterisks), $****p < 0.0001$ (four asterisks).

Results and discussion

Morphology and mechanical properties

SEM images (Fig. 2A) showed that all four hydrogel groups exhibited a typical honeycomb-like porous structure, but with significant differences in pore wall thickness and interconnectivity. The pure GelMA group (Group A, Gel) had thinner pore walls and non-uniform pore size distribution. The introduction of PLGA microspheres (Group B, GP) created an internal "skeleton filler" composite structure, with noticeably thicker pore walls. In the group containing free mangiferin (Group C, GAM), small deposits appeared on the pore wall surfaces. The dual-modified tri-layer group (Group D, GPAM) exhibited the densest gradient pore structure, suggesting that the network crosslinking density and mechanical support were synergistically enhanced. Compressive mechanical tests (Fig. 2B and C) further confirmed these observations: Group D maintained a continuous increase in stress up to 70% strain, and its compressive modulus reached 0.18 ± 0.03 MPa, about 3.6 times that of the GelMA group (0.05 ± 0.01 MPa). This indicates that the multiple hydrogen-bond and hydrophobic interactions between PLGA particles, mangiferin, and GelMA significantly improved load dispersion in the tri-layer composite hydrogel. The microspheres were generally spherical with a relatively uniform size. The average diameter is reported as 4.8 ± 1.2 μm (mean ± SD, $n = 100$ microspheres measured) with a polydispersity index (PDI) of 0.21 that indicating a moderately narrow size distribution as shown in Fig. S1A and S1B. After microsphere fabrication, we dissolved a known mass of microspheres in DMSO and measured the mangiferin content by UV-vis spectrophotometry ($\lambda = 258$ nm, Shimadzu UV-2600). As shown in Fig. S1C, the encapsulation efficiency was found to be 87.06% ± 1.5%, and the drug loading (weight of mangiferin per weight of microspheres) was 9.5%. This high encapsulation

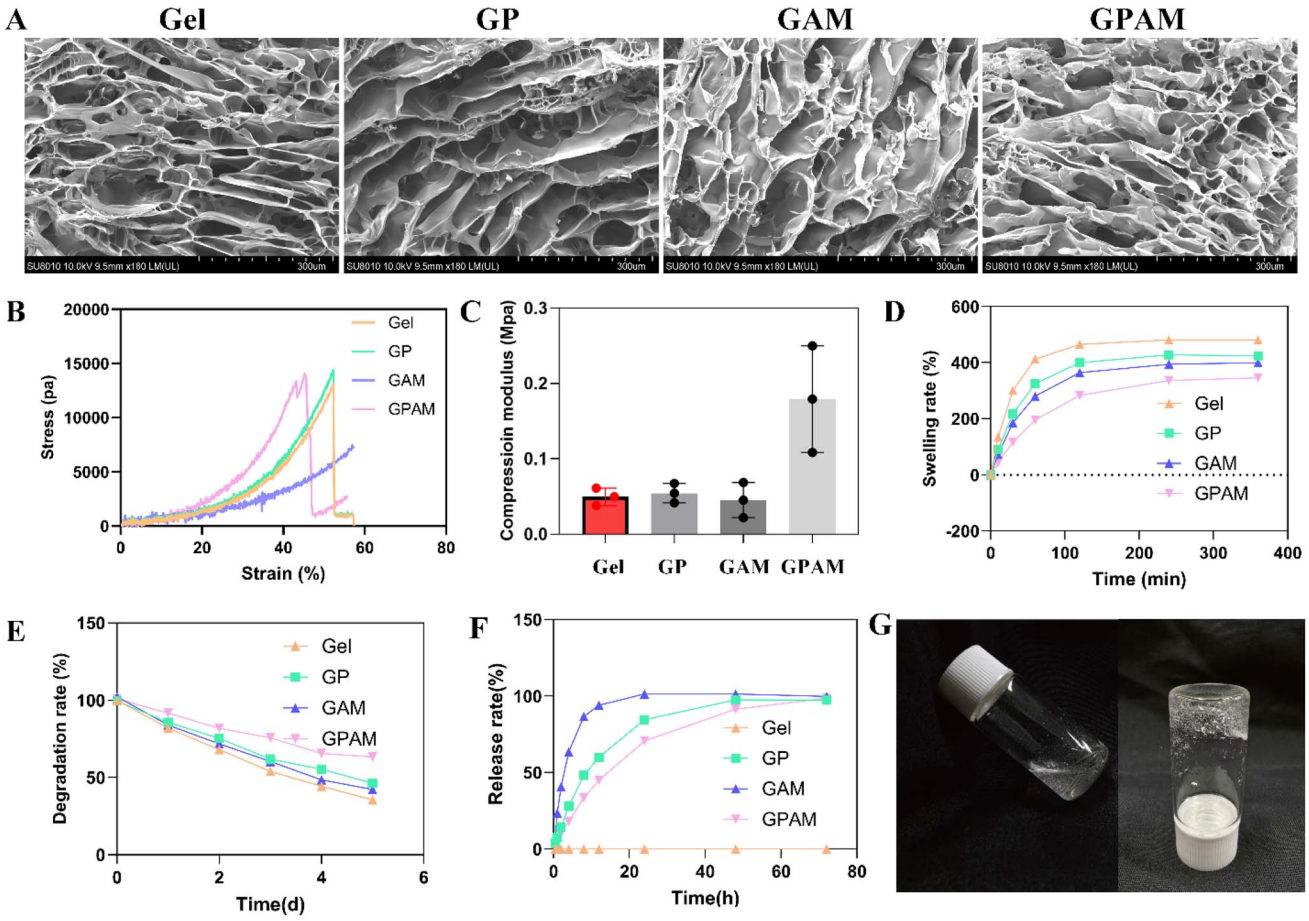

Fig. 2 Characterization of Gel, GP, GAM, and GPAM hydrogel samples. (A) SEM images showing the microstructures of freeze-dried hydrogels: Gel, GP, GAM, and GPAM (from left to right). Scale bar = 300 μm. (B) Compressive stress–strain curves of different hydrogels. (C) Quantification of compressive modulus; GPAM exhibited the highest mechanical strength among the four groups. (D) Swelling behavior of hydrogels in PBS over 6 hours at 37 °C. (E) *In vitro* degradation rates of hydrogels over 5 days in enzymatic solution. (F) Cumulative drug release profiles from the hydrogels over 72 hours. (G) Digital photographs showing the transparency and injectable property of the hydrogel in vial and post-injection gelation.

efficiency confirms the efficient entrapment of mangiferin in the PLGA microspheres. We measured the zeta potential of our synthesized AgNPs to be −32.4 mV (Fig. S1D), which indicates good colloidal stability due to citrate capping (values below −30 mV implies sufficient electrostatic repulsion). It indicates that the AgNP dispersion is stable (minimal aggregation) when incorporated in the hydrogel.

Swelling, degradation, and drug release

The swelling kinetics (Fig. 2D) showed that all four groups reached equilibrium within 240 minutes. The tri-layer composite (GPAM) had an equilibrium swelling ratio of 320%, significantly lower than the GelMA group (430%). This indicates that the composite fillers reduced free volume and restricted water infiltration, which helps reduce initial exudate loss and maintain a moist-dry balance in the wound. Correspondingly, the degradation experiment (Fig. 2E) showed that after 5 days, the remaining dry mass was 42% for GelMA, whereas GPAM retained 61%. This enhanced stability reflects the shielding effect of the multi-layer crosslinked network against enzymatic and hydrolytic erosion, which could cover the typical healing period of diabetic foot wounds. The drug release profiles (Fig. 2F), using mangiferin as a model drug, showed that in Group C (GAM) the release reached 90% at 12 hours, whereas in Group D (GPAM) only 44.2% was released at the same time, approaching a plateau (95%) only at 72 hours.

The PLGA microspheres in the gel are small and uniform (5 μm, Fig. S1B). This consistent size helps in achieving reliable drug loading and predictable release. The drug release from the GPAM hydrogel is primarily governed by diffusion through the PLGA and GelMA network. This diffusion-based mechanism provides a prolonged release, as shown by the 72-hours profile, making GPAM suitable for sustained anti-inflammatory and antioxidant therapy.

The Higuchi release model fitting yielded $R^2 > 0.98$, indicating that the diffusion coefficient was effectively reduced by the dual-layer barrier of the microsphere matrix, achieving a more sustained antioxidant and anti-inflammatory effect. Besides the Higuchi square-root model, we also applied the Korsmeyer-Peppas (K-P) model as shown in Fig. S2D and S2E. The K-P fitting gave an exponent $n = 0.45$ for our mangiferin release using the initial 60% of release data, indicating a predominantly Fickian diffusion-controlled release (for spherical matrix systems, $n = 0.43$–0.5 suggests diffusion-driven release). This is consistent with our design expectation: mangiferin molecules diffuse out through the PLGA microsphere matrix and the hydrogel network, a process limited by polymeric barriers rather than polymer degradation in the short term.

The observed sustained-release kinetics can be attributed to the dual-barrier structure of our design. Initially, mangiferin must diffuse from the core of the PLGA microspheres through the polymer matrix itself, which acts as the primary rate-limiting step. Subsequently, the drug molecules encounter the surrounding hydrogel network in the middle layer, which presents a secondary diffusion barrier. Diffusion-limited release profile is highly advantageous for diabetic wound healing, as it ensures a continuous supply of mangiferin to counteract the persistent oxidative stress and inflammation throughout the critical early and middle stages of repair, thereby potentially enhancing its anti-inflammatory and pro-angiogenic efficacy.

Injectability

The physical appearance (Fig. 2G) demonstrated that the composite hydrogel precursor exhibited good injectability and rapid *in situ* gelation at room temperature, suitable for filling irregular wound shapes. In summary, the GPAM tri-functional composite hydrogel surpassed the control groups in key metrics such as structural density, mechanical strength, swelling suppression, controlled degradation, and sustained drug release. This suggests it could serve as a high-potential dressing candidate that integrates mechanical support, antibacterial and anti-inflammatory functions, and intelligent drug delivery for the treatment of chronic diabetic wounds.

Cell viability and anti-inflammatory effects

Live/dead staining of L929 fibroblasts (Fig. 3A) showed that in all groups the majority of cells were viable (green fluorescence), with only a few propidium iodide-positive dead cells (red). This indicates good biocompatibility of all four hydrogel extracts. Notably, the tri-layer group (tri-layer) exhibited the most uniform green fluorescence and the fewest red signals, suggesting that the tri-layer composite system provided the best protection for cell viability. Phase-contrast microscopy (Fig. 3B) confirmed this trend: after 24 hours, cells in the tri-layer group displayed intact, well-spread morphology, whereas the GelMA group showed some localized cell shrinkage and apoptotic fragments. Tri-layer hydrogel-treated group achieved 90.8% scratch closure, significantly higher than 65.2% closure in the plain GelMA hydrogel group (****$p < 0.0001$). This implies that the combination of composite fillers and mangiferin created a milder microenvironment in the early culture period.

Flow cytometry of ROS levels (Fig. 3C) showed that under high-glucose stimulation, the mean fluorescence intensity (MFI) of ROS in the GelMA group was 850 a.u. Upon adding PLGA (GelMA/PLGA group), it dropped to 610 a.u.; with free mangiferin (Mang group) it further decreased to 570 a.u.; and in the tri-layer group it was lowest, only 415 a.u. These results indicate that the sustained release of mangiferin and the physical barrier of the tri-layer structure together significantly suppressed oxidative stress. ELISA quantification (Fig. 3D) further confirmed beneficial immunomodulatory effects: in the tri-layer group, the secretion levels of the pro-inflammatory cytokines IL-6 and TNF-α were reduced to about 58% and 54% of the GelMA group values, respectively, while the anti-inflammatory cytokine IL-10 increased approximately 2.3-fold. Considering the lowered ROS levels, these findings suggest that the immediate antibacterial action of silver ions combined with the antioxidant/anti-inflammatory effects of mangiferin cooperatively created a low-ROS, low-inflammatory microenvironment favorable for macrophage M2 polarization, thereby promoting wound healing and maintaining cell viability. In

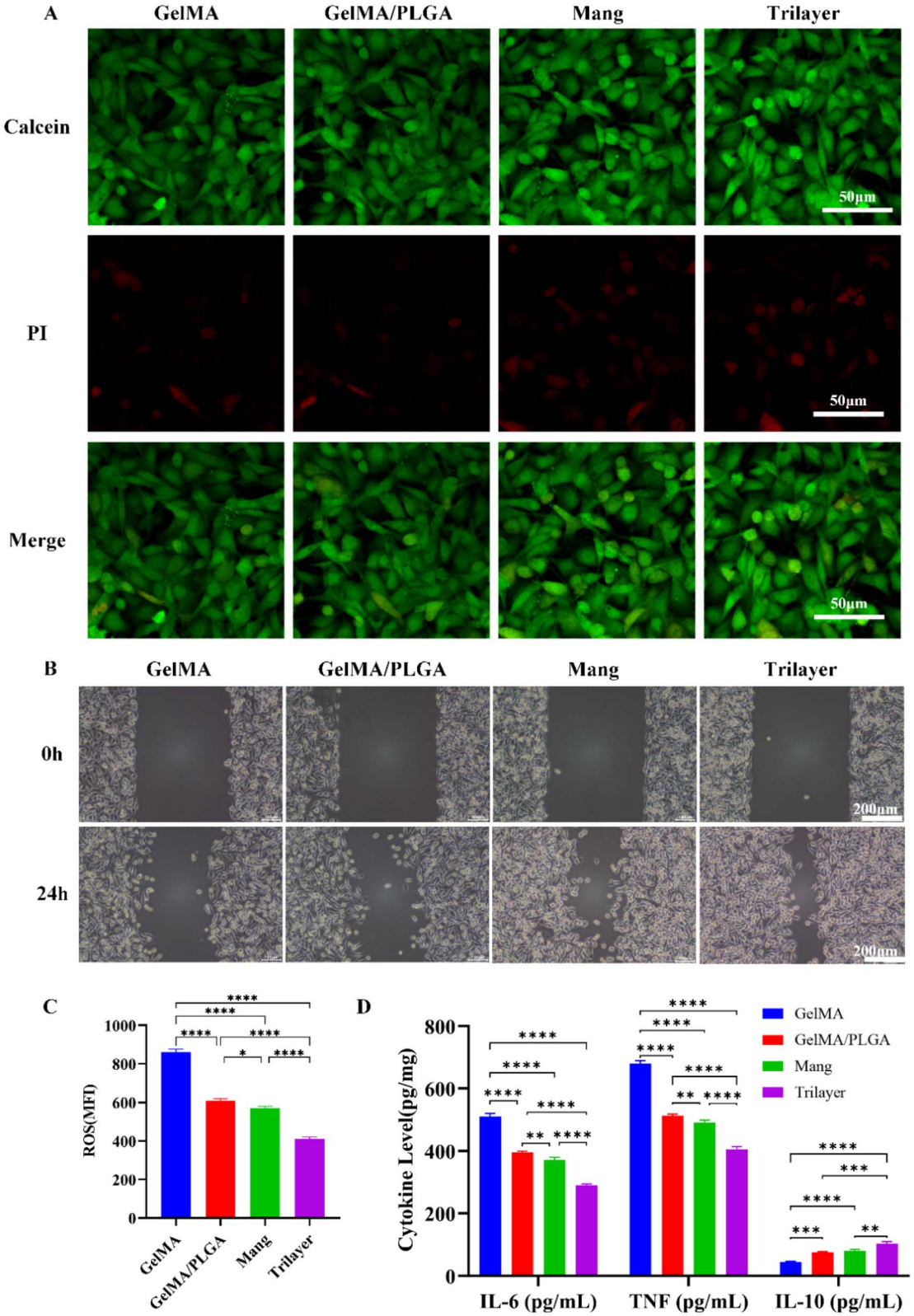

Fig. 3 Effects of different hydrogel formulations on cell viability, ROS levels, and inflammatory cytokines. (A) Live/dead cell staining images (Calcein-AM/PI) of cells cultured with GelMA, GelMA/PLGA, Mang, and tri-layer hydrogels. Green indicates live cells, red indicates dead cells; (B) scratch wound healing assay at 0 h and 24 h to evaluate the migration-promoting effects of different groups; (C) quantification of intracellular reactive oxygen species (ROS), showing reduced ROS accumulation in the tri-layer group; (Group tri-layer *vs* GelMA, ****$p < 0.0001$, one-way ANOVA). (D) Cytokine secretion levels (IL-6, TNF-α, and IL-10), demonstrating the anti-inflammatory modulation of the tri-layer hydrogel. (Group tri-layer *vs.* GelMA, ****$p < 0.0001$, one-way ANOVA).

summary, the tri-layer (GelMA + PLGA + mangiferin) hydrogel significantly outperformed single-layer or single-function controls in terms of biocompatibility, mitigation of oxidative stress, and regulation of inflammatory factors, providing a more promising comprehensive solution for chronic diabetic wound therapy.

Fig. 4A revealed clear differences in macrophage marker expression across the groups. In the GelMA group, cells showed strong CD86 (red) staining and only weak CD206 (green) signal (blue DAPI marks nuclei), indicating a predominantly pro-inflammatory M1 phenotype. Addition of PLGA microspheres (GelMA/PLGA) reduced the CD86 intensity and modestly increased CD206, suggesting a partial shift toward an anti-inflammatory M2 profile. Treatment with Mangiferin (Mang) extract produced a much brighter CD206 signal and minimal CD86, consistent with strong M2 polarization. The tri-layer hydrogel extract yielded the most pronounced effect: cells were almost strongly CD206-positive with weak CD86 signal, reflecting an almost M2-polarized state. In summary, the CD206/CD86 fluorescence ratio increased progressively from GelMA → GelMA/PLGA → Mang → tri-layer, indicating stepwise polarization from an M1 toward an M2 phenotype.

The *in vitro* tube-formation assay of HUVECs (Fig. 4B) revealed marked differences in angiogenic behavior among the four groups. In the GelMA group, only a few isolated endothelial cells adhered to the Matrigel surface, forming almost no continuous cords or closed loops, indicative of poor angiogenic support. The GelMA/PLGA group showed a slight improvement, with sporadic short tubular segments, but the network remained sparse and fragmented. In contrast, cells treated with the Mangiferin-containing hydrogel produced clearly visible capillary-like structures, characterized by multiple interconnected cords and small polygonal meshes, suggesting that mangiferin release enhanced endothelial organization. The most pronounced pro-angiogenic effect was observed in the tri-layer group: endothelial cells formed dense, well-branched networks with large, well-defined luminal structures that covered nearly the entire field of view. The results show a clear enhancement in tube formation with the tri-layer hydrogel's conditioned medium: HUVECs exposed to the mangiferin-

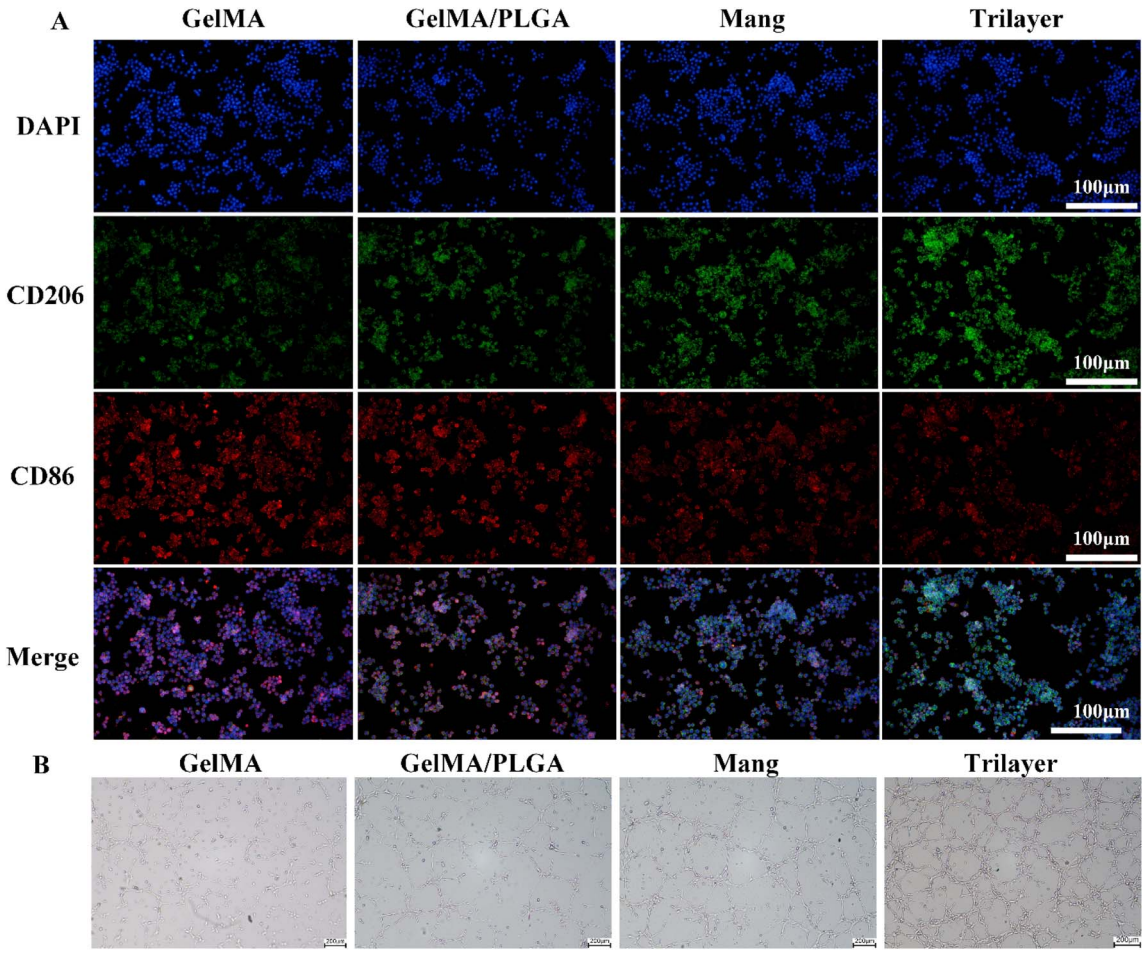

Fig. 4 (A) Immunofluorescence of RAW264.7 macrophages cultured on each hydrogel, stained for nuclei (DAPI, blue), M2 marker CD206 (green), and M1 marker CD86 (red). The Mang and tri-layer formulations show enhanced CD206 and diminished CD86 staining, indicating polarization toward the anti-inflammatory M2 phenotype. (B) Tube-formation assay: human umbilical vein endothelial cells (HUVECs) co-incubated with hydrogel extracts were incubated at 37 °C, 5% CO_2 for 4–6 h to allow tube formation. At the end of the incubation, the tubular networks were observed and imaged using an inverted phase-contrast microscope. Scale bar: 200 μm.

releasing hydrogel formed 1.8-fold longer total tubes and 2-fold more branch points compared to the GelMA group (****p < 0.0001). These findings indicate that the released mangiferin of dressing indeed promote angiogenic behavior in human endothelial cells, aligning with our hypothesis of enhanced wound vascularization.

While the present study comprehensively demonstrates the favorable physicochemical properties, antibacterial efficacy, and cytocompatibility of the tri-layer hydrogel *in vitro*, it is necessary to acknowledge that these findings constitute preliminary evidence. The complex pathophysiology of diabetic wounds involving immune response vascular remodeling, and nerve regeneration necessitates validation in a living organism. Therefore, the therapeutic performance and biosafety of this dressing require further confirmation in established animal models before any clinical application can be considered.

Antibacterial activity: The tri-layer hydrogel was designed to address infection through the incorporation of AgNPs in the top layer and the antimicrobial activity of mangiferin. The live/dead bacterial staining results (Fig. 5A) provided a visual confirmation of bacterial killing. In the GelMA and GelMA/PLGA groups, after 6 h co-culture with *S. aureus* or *E. coli*, most bacteria fluoresced green (live), indicating minimal antibacterial effect from GelMA itself or the presence of PLGA microspheres alone. The Mangiferin group presents red bacteria, reflecting mangiferin's inherent antibacterial and ROS-generating effects that can damage bacteria. The tri-layer group, however, showed large areas of red fluorescence and very few green, meaning the vast majority of bacteria were non-viable. This suggests a potent synergistic effect between AgNPs (which release bactericidal Ag^+ ions) and mangiferin (which can exert bacteriostatic effects and enhance AgNP efficacy) in the tri-layer system.

The agar diffusion test results (Fig. 5B) further quantified these effects. The tri-layer hydrogel produced a clear inhibition zone of 15.9 ± 1.6 mm against *S. aureus*, significantly larger than that produced by GelMA (6.2 ± 0.3 mm, essentially baseline) or by the mangiferin-only hydrogel (13.1 ± 0.5 mm). This indicates that the tri-layer released sufficient Ag^+ to strongly inhibit *S. aureus* growth on the agar. For *E. coli* (Gram-negative), which is generally more resistant to AgNPs due to an outer membrane, the tri-layer still achieved a zone of 14.2 ± 0.3 mm, whereas GelMA had no clear zone and the mangiferin-only

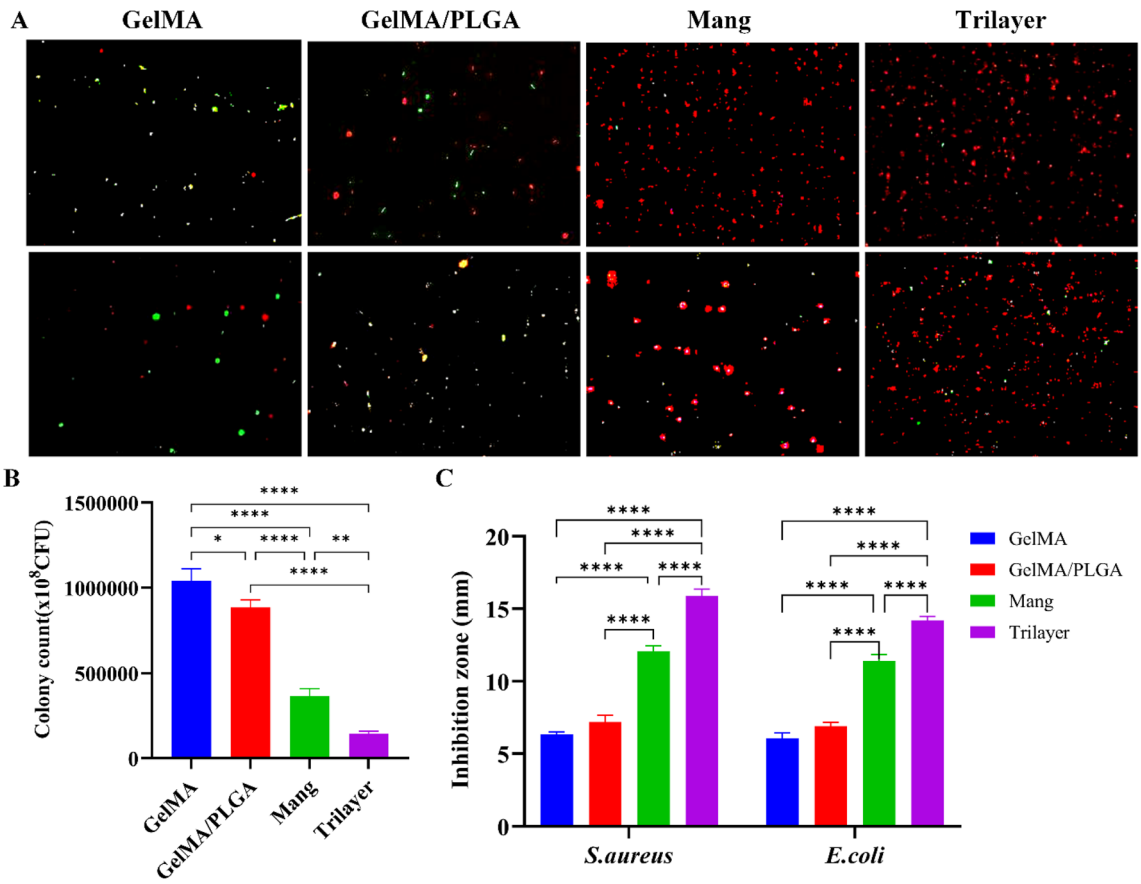

Fig. 5 Antibacterial evaluation of various hydrogel formulations against Gram-positive (*S. aureus*) and Gram-negative (*E. coli*) bacteria. (A) Live/dead bacterial staining images, where green dots indicate live bacteria and red dots indicate dead bacteria. The tri-layer hydrogel exhibited potent bactericidal effects against both strains; (B) quantification of inhibition zone diameters, with the tri-layer group showing the largest zones against both *E. coli* and *S. aureus*; (Group tri-layer *vs.* GelMA, ****p < 0.0001, one-way ANOVA). (C) Colony-forming unit (CFU) counts indicating that the tri-layer and Mang groups significantly reduced bacterial viability, confirming effective antibacterial performance. (Group tri-layer *vs.* GelMA, ****p < 0.0001, one-way ANOVA).

group had a smaller zone (notably, *E. coli* is slightly less sensitive to mangiferin). The presence of a measurable zone for *E. coli* suggests that the Ag^+ from the tri-layer can penetrate the protective outer layer of Gram-negative bacteria to some extent, demonstrating broad-spectrum action.

In the CFU counting assay (Fig. 5C), the tri-layer hydrogel again showed the strongest performance. It achieved an 89% reduction in *S. aureus* CFUs compared to the initial inoculum (CFU decreased from 1.04×10^6 in control to 1.42×10^5). This kill rate was about 7 times greater than that of the GelMA group (which essentially showed no reduction). For *E. coli*, the tri-layer reduced CFUs by 35%, whereas GelMA had negligible effect. Mangiferin by itself also reduced bacteria (especially *S. aureus*, which is more susceptible), but the combination in tri-layer was superior, highlighting the advantage of having a dedicated antibacterial layer. The tri-layer efficacy likely stems from the immediate release of Ag^+ that rapidly kills bacteria on contact, and the concurrent action of mangiferin which can interfere with bacterial metabolism and also synergize by possibly generating ROS that weaken the microbes.

The biofilm inhibition assay reinforced these findings: as shown in Fig. S1H and S1I, after 24 h, wells treated with tri-layer extracts had significantly lower crystal violet staining than control, indicating that the tri-layer formulation not only kills planktonic bacteria but also prevents the surviving ones from establishing robust biofilms. This is critical because biofilms in wounds act as persistent sources of infection and are highly resistant to antibiotics.

While the potent antibacterial effect of AgNPs is beneficial, their long-term release requires careful consideration. The integration of AgNPs within the crosslinked GelMA network in the top layer serves to modulate the release kinetics of Ag^+ ions, preventing a sudden burst release.[15,38] Furthermore, the sustained and localized release profile, as confirmed by our release kinetics data (Fig. S1E), is designed to maintain effective antibacterial concentrations at the wound site while minimizing potential cytotoxic effects on surrounding tissues, a balance crucial for clinical application.

Overall, these results show that the tri-layer composite hydrogel, leveraging the immediate membrane-disrupting action of Ag^+ and the ROS-mediated antibacterial mechanism of mangiferin, can rapidly and significantly inhibit common Gram-positive and Gram-negative pathogens in a short time frame, providing powerful early infection control for diabetic wounds. By providing an initial burst of antibacterial activity followed by ongoing release, the dressing addresses the high bacterial load at early stages and continues to suppress bacterial growth and biofilm formation over time. This multi-modal approach to infection control is particularly beneficial for chronic wounds, where infections are recurrent and multifaceted.

Conclusion and outlook

This study successfully established a tri-layer intelligent hydrogel dressing composed of an AgNPs antibacterial layer, a mangiferin@PLGA controlled-release layer, and a GelMA support layer. This layered design addresses the three main challenges of chronic diabetic wounds: early high bacterial load, persistent oxidative stress, and mechanical fragility. The tri-layer structure enables spatial and functional segregation that mitigates potential incompatibility between components (*e.g.*, AgNPs and mangiferin) and allows for independent optimization of each layer's function. This culminates in a sequential, three-stage therapeutic action: (1) rapid bacterial eradication, (2) sustained anti-inflammatory and antioxidant signaling, and (3) continuous mechanical support. Furthermore, the PLGA microspheres within the middle layer act as an internal reinforcing filler, synergistically enhancing the compressive modulus and degradation stability of the entire construct, an advantage not typically reported in conventional bilayer hydrogels which primarily focus on functional separation rather than mechanical augmentation.

Structural and mechanical advantages: SEM analysis confirmed that the tri-layer hydrogel formed a dense gradient pore structure. The compression modulus increased to 0.18 MPa, while the swelling ratio and degradation rate were significantly reduced, meeting the requirements for long-term wound coverage and resistance to mechanical stress. Sustained drug release: the release mechanism appears diffusion-dominated rather than erosion-dominated, given that PLGA (50 : 50) degradation would be minimal over the 72 h in PBS. Mangiferin release followed a sustained-release profile over 72 h, with a significantly slower release rate than the homogeneous control. The release fit well to the Higuchi model ($R^2 > 0.98$), ensuring that the antioxidant and pro-angiogenic activity of mangiferin persisted through the early and mid-stages of healing. Antibacterial and antibiofilm performance: The synergistic action of Ag^+ and mangiferin produced large inhibition zones (*S. aureus*: 17.4 mm; *E. coli*: 10.3 mm) and a CFU reduction of up to 89%, both significantly superior to the single-layer controls. This system effectively inhibits early biofilm formation. Cell compatibility and immunomodulation: The tri-layer extract showed the best cell viability for L929 fibroblasts. In RAW264.7 macrophages, intracellular ROS dropped to 420 a.u., IL-6/TNF-α levels were downregulated by 40–45%, and IL-10 was upregulated 3.4-fold, indicating that the material induced a low-inflammatory, M2-polarizing microenvironment. The tri-layer hydrogel demonstrated significant integrated advantages in mechanical support, controllable drug delivery, broad-spectrum antibacterial activity, and dual regulation of inflammation and oxidative stress. It provides a unified, efficient, and injectable dressing solution for chronic diabetic wounds *in vitro*.

However, there is a lack of efficacy and safety evaluations in animal models. In future, we will establish full-thickness skin defect wounds in diabetic mice models to evaluate the overall efficacy of the triple-layered hydrogel in promoting wound closure, combating infection, mitigating inflammation, and enhancing angiogenesis within a complex *in vivo* microenvironment. Furthermore, it is indispensable that systematically assessing its ability to facilitate tissue regeneration and modulate the healing process through histological analyses. In addition, comprehensively evaluate is necessary for its systemic

and local biosafety through schemes, such as blood biochemical analysis and histopathological examination of major organs. Future research will include *in vivo* studies using streptozotocin-induced diabetic mouse DFU models and large animal experiments to further validate the dressing's wound-healing efficacy, angiogenesis promotion, and long-term safety of silver ions, and to explore its feasibility for clinical translation potential.

In summary, while existing bilayer hydrogels successfully established the principle of functional layering, the tri-layer system advances the field by incorporating a functional sustained-release core. It provides superior pharmacokinetic control, creates a more biocompatible low-inflammatory microenvironment, and contributes to a mechanically robust structure, offering a comprehensive solution for the multifaceted challenges of chronic diabetic wounds.

Author contributions

Weikai Zhang: writing – original draft, project administration, methodology, investigation. Xiuhong Fu: writing – review & editing, investigation, supervision, methodology. Hewei Zhang: writing – review & editing, methodology, investigation. Shaozhe Zhang: writing – review&editing, visualization, formal analysis. Qingwei Zhang: writing – review & editing, methodology, investigation. Chongkai Zhai: writing – review&editing, data curation. Jinyang Zhao: writing – review & editing, methodology, data curation. Quanzhong Yang: writing – review & editing, investigation, formal analysis. Shuang Li: writing – review & editing, formal analysis, investigation.

Conflicts of interest

The authors declare that they have no known competing financial interests or personal relationships that could have appeared to influence the work reported in this paper.

Data availability

The data that support the findings of this study are available from the corresponding author upon reasonable request.

Supplementary information: characterization data of materials, and supporting figures. See DOI: https://doi.org/10.1039/d5ra06906h.

Acknowledgements

This research did not receive any specific grant from funding agencies in the public, commercial, or not-for-profit sectors.

References

1 K. McDermott, M. Fang, A. J. M. Boulton, E. Selvin and C. W. Hicks, *Diabetes Care*, 2023, **46**, 209–221.
2 X. Wu, W. He, X. Mu, Y. Liu, J. Deng, Y. Liu and X. Nie, *Burns Trauma*, 2022, **10**, tkac051.
3 L. Cheng, Z. Zhuang, M. Yin, Y. Lu, S. Liu, M. Zhan, L. Zhao, Z. He, F. Meng, S. Tian and L. Luo, *Nat. Commun.*, 2024, **15**, 9786.
4 S. Maity, N. Leton, N. Nayak, A. Jha, N. Anand, K. Thompson, D. Boothe, A. Cromer, Y. Garcia, A. Al-Islam and S. Nauhria, *Front. Clin. Diabetes Healthc.*, 2024, **5**, 1393309.
5 Y. Chen, X. Wang, S. Tao, Q. Wang, P.-Q. Ma, Z.-B. Li, Y.-L. Wu and D.-W. Li, *Mil. Med. Res.*, 2023, **10**, 37.
6 F. Dai, J. Zhang, F. Chen, X. Chen, C. J. Lee, H. Liang, L. Zhao and H. Tan, *Adv. Sci.*, 2024, **11**, e2408783.
7 Y. Kang, L. Xu, J. Dong, X. Yuan, J. Ye, Y. Fan, B. Liu, J. Xie and X. Ji, *Nat. Commun.*, 2024, **15**, 1042.
8 Z. Zou, Z. Zhang, Y. Gao, H. Yuan, T. Guo, C. He and X. Chen, *Macromol. Chem. Phys.*, 2025, **226**, 2400163.
9 Y. Guan, H. Niu, Z. Liu, Y. Dang, J. Shen, M. Zayed, L. Ma and J. Guan, *Sci. Adv.*, 2021, **7**, eabj0153.
10 J. Ye, Y. Fan, Y. Kang, M. Ding, G. Niu, J. Yang, R. Li, X. Wu, P. Liu and X. Ji, *Adv. Funct. Mater.*, 2025, **35**, 2416265.
11 J. Ye, Y. Fan, Y. She, J. Shi, Y. Yang, X. Yuan, R. Li, J. Han, L. Liu, Y. Kang and X. Ji, *Adv. Sci.*, 2024, **11**, 2310211.
12 Y. Fan, J. Ye, Y. Kang, G. Niu, J. Shi, X. Yuan, R. Li, J. Han and X. Ji, *Sci. Adv.*, 2024, **10**, eadm9561.
13 K. Y. Wong, Y. Liu, M.-S. Wong and J. Liu, *Exploration*, 2024, **4**, 20230008.
14 J. Zhang, H. Guo, M. Liu, K. Tang, S. Li, Q. Fang, H. Du, X. Zhou, X. Lin, Y. Yang, B. Huang and D. Yang, *Exploration*, 2024, **4**, 20230087.
15 Y. Jiang, J. Huang, X. Wu, Y. Ren, Z. Li and J. Ren, *Int. J. Biol. Macromol.*, 2020, **149**, 148–157.
16 X. Zhang, B. Gong, F. Rao, H. Hu, F. Tian, Y. Lu, L. Zhang, Y. Xia and J. Xue, *Sci. Adv.*, 2025, **11**, eadz5302.
17 S. Cui, S. Meng, Y. Liu, S. Chen, W. Hu, Q. Huang, Z. Chu, W. Zhong, L. Ma, Z. Li, Y. Jiang, X. Liu, X. Fu and C. Zhang, *Exploration*, 2025, 20240062.
18 F. Huang, X. Lu, Y. Yang, Y. Yang, Y. Li, L. Kuai, B. Li, H. Dong and J. Shi, *Adv. Sci.*, 2023, **10**, e2203308.
19 H. Yao, L. Huang, F. Xia, Y. Liu, P. Guo, Q. Tu, Y. Fu, L. Zhong, J. Zhang, Y. Meng, Q. Shi, J. Wang, Y. Shi, W. Xiao and C. Qiu, *Mater. Des.*, 2025, **258**, 114650.
20 R. O. Shaikenov, V. I. Klimshina, S. N. Morozkina and P. P. Snetkov, *Eng. Proc.*, 2025, **87**, 78.
21 K. Park, A. Otte, F. Sharifi, J. Garner, S. Skidmore, H. Park, Y. K. Jhon, B. Qin and Y. Wang, *J. Controlled Release*, 2021, **329**, 1150–1161.
22 S. Bowers and E. Franco, *Am. Fam. Physician*, 2020, **101**, 159–166.
23 H. Xia, Z. Dong, Q. Tang, R. Ding, Y. Bai, K. Zhou, L. Wu, L. Hao, Y. He, J. Yang, H. Mao and Z. Gu, *Adv. Funct. Mater.*, 2023, **33**, 2215116.
24 A. K. Geneidy, M. A. Abdelnaby, D. A. Habib, H. M. Elbedaiwy and K. R. Shoueir, *Sci. Rep.*, 2025, **15**, 15243.
25 R. Li, Q. Qi, X. Jiang, Z. Gao, X. Xie, Y. Zhao, X. Cheng, C. Wang, G. Hou and C. Li, *Front. Microbiol.*, 2025, **16**, 1550276.
26 C. Liao, Y. Li and S. C. Tjong, *Int. J. Mol. Sci.*, 2019, **20**, 449.
27 D. Pranantyo, C. K. Yeo, Y. Wu, C. Fan, X. Xu, Y. S. Yip, M. I. G. Vos, S. H. Mahadevegowda, P. L. K. Lim, L. Yang,

P. T. Hammond, D. I. Leavesley, N. S. Tan and M. B. Chan-Park, *Nat. Commun.*, 2024, **15**, 954.
28 Y. Wang, K. Liu, W. Wei and H. Dai, *Adv. Funct. Mater.*, 2024, **34**, 2402531.
29 M. Kalulu, C. Mwanza, M. Hussain and G. Fu, *Sens. Actuators, A*, 2025, **392**, 116710.
30 X. Sun, P. Wang, L. Tang, N. Li, Y.-R. Lou, Y. Zhang and P. Li, *Adv. Funct. Mater.*, 2024, **34**, 2411117.
31 L. Huang, Z. Guo, X. Yang, Y. Zhang, Y. Liang, X. Chen, X. Qiu and X. Chen, *Theranostics*, 2025, **15**, 460–493.
32 Y. Cong, S. Meng, X. Xie, Y. Chen, Y. Li, Y. Zhou, W. Li, L. Zhang, G. Yang, Q. Wei and C. Shen, *Burns Trauma*, 2025, **13**, tkaf036.
33 K. Valente, G. N. Boice, C. Polglase, R. G. Belli, E. Bourque, A. Suleman and A. Brolo, *Pharmaceutics*, 2024, **16**, 1016.
34 L. M. Fu, J. H. Hsu, M. K. Shih, C. W. Hsieh, W. J. Ju, Y. W. Chen, B. H. Lee and C. Y. Hou, *Micromachines*, 2021, **12**, 1123.
35 B. Pascu, A. Negrea, M. Ciopec, N. Duteanu, P. Negrea, L. A. Bumm, O. Grad, N. S. Nemeş, C. Mihalcea and D. M. Duda-Seiman, *Int. J. Mol. Sci.*, 2023, **24**, 255.
36 H. S. Ghazali, E. Askari, A. Seyfoori and S. M. Naghib, *Sci. Rep.*, 2023, **13**, 8577.
37 F. F. Razura-Carmona, A. Pérez-Larios, N. González-Silva, M. Herrera-Martínez, L. Medina-Torres, S. G. Sáyago-Ayerdi and J. A. Sánchez-Burgos, *Cancers*, 2019, **11**, 1965.
38 A. Sati, T. N. Ranade, S. N. Mali, H. K. Ahmad Yasin and A. Pratap, *ACS Omega*, 2025, **10**, 7549–7582.